LANGMUIR

pubs.acs.org/Langmuir Article

# Water Content in Nanoparticles Determined by Small-Angle Neutron Scattering and Light Scattering

Behrad Kangarlou,[▽] Donyeil Hoy,[▽] Haden L. Scott, Sai Venkatesh Pingali, Nora Khalil, Benjamin Chung, John Katsaras, and Mu-Ping Nieh*

Cite This: *Langmuir* 2023, 39, 227−235 Read Online

ACCESS | Metrics & More | Article Recommendations | Supporting Information

Downloaded via UNIV OF CONNECTICUT on July 1, 2023 at 21:57:43 (UTC).
See https://pubs.acs.org/sharingguidelines for options on how to legitimately share published articles.

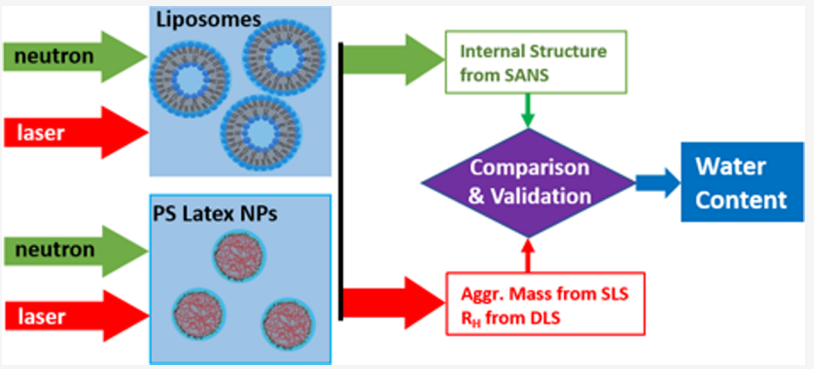


**ABSTRACT:** The amount of water in therapeutic nanoparticles (NPs) is of great importance to the pharmaceutical industry, as water content reflects the volume occupied by the solid components. For example, certain biomolecules, such as mRNA, can undergo conformational change or degradation when exposed to water. Using static light scattering (SLS) and dynamic light scattering (DLS), we estimated the water content of NPs, including extruded liposomes of two different sizes and polystyrene (PS) Latex NPs. In addition, we used small-angle neutron scattering (SANS) to independently access the water content of the samples. The water content of NPs estimated by SLS/DLS was systematically higher than that from SANS. The discrepancy is most likely attributed to the larger radius determined by DLS, in contrast to the SANS-derived radius observed by SANS. However, because of low accessibility to the neutron facilities, we validate the combined SLS/DLS to be a reasonable alternative to SANS for determining the water (or solvent) content of NPs.

## INTRODUCTION

Rational design of nanoparticles (NPs) is an emergent field of research, especially for biomedical applications, such as the delivery of a variety of payloads using nanocarriers. Recent examples of lipid nanoparticles (LNPs) used as COVID-19 vaccines encapsulate fragile messenger RNA (mRNA) and show great potential for the use of new vaccines and as drug delivery agents.[1−4] However, there remain many challenges regarding their controlled formation, stability, and organization, which ultimately affect their performance. For example, the propensity of mRNA to be hydrolyzed, thus reducing its efficacy, highlights the need to know the amount of water content associated with the LNPs.[5,6] One important issue to be resolved is the organization of mRNA with surrounding species in the LNPs. Although high-resolution transmission electron microscopy (TEM) and scanning electron microscopy (SEM) provide detailed images of LNPs, the internal structure cannot be easily resolved. Furthermore, since these techniques only sample a few nanoparticles, the data may not be representative of the bulk LNPs.[7,8] Importantly, however, the water content of LNPs provides indirect information of the possible conformation of the entrapped mRNA. Quartz crystal microbalance (QCM) can be applied for measuring small mass difference[9−12] but cannot identify the volume fraction of the solvent entrapped inside the particles.

Small-angle neutron scattering and small-angle X-ray scattering (SANS and SAXS, respectively) have been employed to probe the internal structure of LNPs. For instance, SAXS has been used to resolve the bilayer structure and particle size of siRNA-containing LNPs together with the help of cryogenic transmission electron microscopy (cryo-TEM) and dynamic light scattering (DLS),[13,14] yet information regarding their water content could not be determined. Due to the distinct scattering capability of neutrons to protium (H) and

Received: September 3, 2022
Revised: December 13, 2022
Published: December 29, 2022

ACS Publications © 2022 American Chemical Society

deuterium (D), SANS has become a powerful approach to identify the location of water by a technique commonly known as *contrast variation*. Contrast variation and SANS have been used to estimate the bilayer thickness of unilamellar vesicles (ULVs) of 1,2-dimyristoyl-phosphatidylcholine (DMPC), as well as the number of water molecules associated with the hydrophilic phosphate group using step functions to describe the hydrophilic headgroup and the hydrophobic tails.[15,16] The approach of combining SANS and SAXS data has also been used to resolve the internal structure of different sizes of mRNA-containing LNPs through contrast variation and isotopic labeling of certain molecules making up the LNP.[17] By fitting the neutron scattering length density (SLD or $\rho_N$) value of the LNP's core and knowing the $\rho_N$ of the LNP's different components and their volume fractions, the core water content (volume fraction of water inside the core) was estimated to be 24%.

Although the water content of NPs can be obtained using SANS, access to neutron scattering facilities is relatively limited, prohibiting researchers from obtaining this important information in a timely manner. Here, our aim is to show that light scattering can be used to provide a reasonable estimate of NP water content. Static light scattering (SLS) is a commonly used technique used to determine the size (i.e., radius of gyration, $R_g$) and the molar mass ($M$) of homogeneously dispersed NPs. SLS with dynamic light scattering (DLS) has been used to estimate the density of microlatex particles.[18−20] However, to the best of our knowledge, light scattering has not been used to estimate water content.

Here, we develop an approach using SLS/DLS to estimate the water content of spherical NPs. Three different NPs, two liposomes, and a polystyrene (PS) latex particle are employed as model systems to validate the methodology, and the results are confirmed by the contrast variation SANS. The SLS/DLS method is more accessible and can be incorporated in quality assurance as a standard protocol of any industrial enterprise to accelerate the discovery of novel LNPs with nontrivial internal structures.

## EXPERIMENTAL SECTION

**Materials.** 1,2-Dimyristoyl-*sn*-glycero-3-phosphocholine (DMPC) and 1,2-dimyristoyl-*sn*-glycero-3-phospho-(1′-rac-glycerol) (sodium salt) (DMPG) were purchased from Avanti Polar Lipids, Inc. and used as supplied. Polystyrene latex nanoparticles (PS60; 60 nm) were purchased from Magsphere, Inc. and used without further purification. $D_2O$ for SANS measurements was purchased from Cambrige Isotope Laboratories, Inc.

**Sample Preparation.** DMPC was doped with DMPG at concentration levels of 0.001 and 0.01 ($\frac{\text{DMPG}}{\text{DMPG + DMPC}}$, defined as $R$) for SLS/DLS and SANS studies, respectively. The anionic lipid, DMPG, which has the same hydrophobic chains as DMPC, was introduced to ensure that there were no multilamellar vesicles (MLVs) in the ULV sample after extrusion.[21] The powdered lipids were dissolved in chloroform and dried under a stream of nitrogen to form a lipid film. The film was placed under vacuum overnight at 50 °C to remove any residual chloroform. The lipid film was then hydrated and thermo-cycled above and below the melting temperature of DMPC, four times before further dilution to yield a solution with a lipid concentration, $C_{lp}$ = 5 mg/mL. The **Lipo-A ULV** stock solution was prepared by extruding the lipid solution at 50 °C through a 50 nm polycarbonate membrane filter (31 passes), followed by an additional extrusion using a 30 nm polycarbonate membrane filter (31 passes). The **Lipo-B ULV** solution was prepared in a similar method but only with a 50 nm filter. It should be noted that the diameter of a ULV is not equal to the nominal pore diameter of the membrane. Instead, it is generally larger. To reduce the data collection time, a higher sample concentration (5.0 mg/mL) was used for SANS experiments, while concentrations of 0.25, 0.50, 0.75, and 1.0 mg/mL were used for SLS/DLS studies. The PS Latex suspensions were diluted from a 100 mg/mL stock suspension to a concentration of 10 mg/mL for SANS measurements. Coulombic repulsion and high concentration will result in an observable structure factor in addition to the form factor of the ULVs. It should be noted that the nonlinear interparticle interaction (structure factor) can be accounted for in SANS analysis but not in the analysis of SLS/DLS data.

Samples with the lower charge density (i.e., $R$ = 0.001) were examined by SLS/DLS to avoid the added complication of interparticle interactions or the structure factor. In the case of SANS, the well-developed Hayter−Penfold mean spherical approximation (H-PMSA) structure factor[22−24] describes the charged interparticle interaction. SANS data were hence simulated by the convolution of a core−shell sphere form factor (Supporting Information) and the H-PMSA structure factor. As such, we chose a higher charge density ($R$ = 0.01) for the SANS samples to minimize the presence of MLVs.

**Differential Refractometer.** A Brookhaven BI-DNDC (New York) with a wavelength, $\lambda$, of 620 nm was used to obtain the refractive index difference ($\Delta n$) between the sample with a known concentration and solvent (reference). By plotting the $\Delta n$ against the sample concentration, $c$, the refractive index increment ($dn/dc$) can be obtained. The experimental outcomes yield 0.3837, 0.1404, and 0.1480 (mL/g) for PS Latex, Lipo-A, and Lipo-B at 30 °C, respectively (Supporting Information, Figure S1). Note that the instrument was first calibrated by KCl/$H_2O$ solutions, which had a known value of $dn/dc$.

**SLS/DLS.** SLS and DLS experiments were conducted using an ALV compact goniometer system (Germany), which has 4 evenly spaced avalanche photodiode detectors (CGS-3MD) and a 22 mW He−Ne laser source with a $\lambda$ = 632.8 nm. The intensity time autocorrelation function was obtained by an ALV-7004 digital multiple tau time-real time correlator, which yielded the field time correlation function. All light scattering tests were conducted at 30 °C.

*Dynamic Light Scattering (DLS).* The intensity time autocorrelation function can be expressed as

$$G^2(\tau) = \frac{\int_0^T I(t)\, I(t+\tau)\, \mathrm{d}t}{T} \tag{1}$$

where T and $\tau$ are the total evaluated time and lag time at a given angle, respectively, and $I(t)$ represents the time-dependent intensity function. The field time autocorrelation function, $g^1(t)$, can be obtained via Siegert relation approximation: $\frac{G^2(\tau)}{\langle I\rangle^2} = (1 + \beta|g^1(t)|^2)$, where $\beta$ and $\langle I\rangle^2$ are, respectively, the coherence factor and square of average intensity. The function $g^1(t)$ should follow an exponential decay, i.e., $e^{-\Gamma\tau}$, where $\Gamma$ is the decay rate. We conducted DLS at four different scattering angles ($\theta$): 36, 68, 100, and 132 degrees (with five runs per angle) and at 30 °C. The translational diffusion coefficient ($D$) was obtained through slope analysis based on $\Gamma = Dq^2$, where $q$ is the scattering vector, expressed as $q = \frac{4\pi n}{\lambda}\sin\left(\frac{\theta}{2}\right)$, with $n$ being the refractive index of the solvent. The hydrodynamic radius ($R_h$) can therefore be obtained via the Stokes−Einstein equation: $R_h = \frac{k_B T}{6\pi\eta D}$, where $k_B$, $T$, and $\eta$ represent the Boltzmann constant, temperature, and viscosity of the solvent, respectively.

*Static Light Scattering (SLS).* SLS samples were prepared at four different concentrations (0.25, 0.5, 0.75, and 1.0 mg/mL) and studied between ∼50 and 120° at 30 °C. The average molar mass ($M$) of the aggregate, radius of gyration ($R_g$), and second virial coefficient ($A_2$) were obtained through analysis of a Zimm plot using eq 2. The higher order terms of concentration ($c$) and angle ($\theta$) were omitted for the low concentration samples and low $q$ limits.


https://doi.org/10.1021/acs.langmuir.2c02420
Langmuir 2023, 39, 227−235

$$\frac{Kc}{R_\theta} = \frac{1}{M}\left(1 + \frac{q^2R_g^2}{3}\right)(1 + 2A_2Mc) \quad (2)$$

$$K = \frac{4\pi^2n^2\left(\frac{dn}{dc}\right)^2}{N_A\lambda^4} \quad (3)$$

where $K$, $c$, and $R_\theta$ are the optical constant, concentration, and Rayleigh ratio (normalized scattered intensity), respectively. In eq 3, $dn/dc$ and $N_A$ denote the refractive index increment and Avogadro's number, respectively. Since both $c$ and $\frac{dn}{dc}$ are determined by the "dry" species alone (i.e., prior to sample preparation), the obtained $M$ should be related to the solvent-excluded NPs.

**Estimation of the Water Content of NPs Using SLS and DLS.** The hypothetical approach of using SLS and DLS is described as follows. For a *spherical* NP, the volume fractions of the dry (prior to the addition of solvent) ($\varphi_{dry}$) and water ($\varphi_{water}$) components can be expressed by the following equations

$$\varphi_{dry} = \frac{V_{dry}}{V_{total}} \quad (4)$$

$$\varphi_{water} = 1 - \varphi_{dry} \quad (5)$$

where $V_{dry}$ and $V_{total}$ denote the volume of the solvent-excluded components and total volume of the NP, respectively, as depicted in Figure 1.

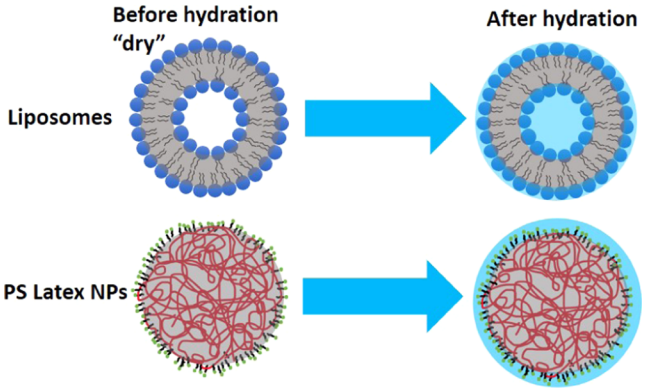


**Figure 1.** Schematics of liposomes and PS Latex NPs in "dry status" (prehydration) and after hydration. The gray color is the hydrophobic region, while the blue color is the hydrated region of each type of NPs. The hydrated region is constituted by the water core and hydrated shell for liposomes and by the outer shell (sulfonated region and surfactants) only for Latex NPs. The obtained values of c and $dn/dc$ are calculated, according to the mass of dry state before hydration on the left.

The molar mass ($M$) of the solvent-excluded NP (in the Static Light Scattering section) was obtained from Zimm plots using SLS measurements. From this, $V_{dry}$ is obtained: $V_{dry} = \frac{M}{\rho N_A}$, where $\rho$ and $N_A$ are the density of the solvent-excluded material and Avogadro's number, respectively. $R_h$ is determined from DLS measurements and can be considered to be the radius of the NP, *assuming a spherical* morphology. The total volume of the nanoparticle can thus be estimated by $V_{total} = \frac{4}{3}\pi R_h^3$, which is then used to calculate $\varphi_{dry}$ and $\varphi_{water}$ using eqs 4 and 5.

**Small-Angle Neutron Scattering (SANS).** SANS data were collected on a CG-3 Bio-SANS instrument at a high flux isotope reactor (HFIR) located at the Oak Ridge National Laboratory.[25] Samples were measured in cylindrical quartz cuvettes (banjo cells) with a 1 or 2 mm pathlength at 32 ± 1 °C. This temperature was chosen for all SLS/DLS and SANS measurements to ensure that all lipids were in the fluid phase (the melting transition temperatures of DMPC and DMPG are around 24 °C). Therefore, the liposomes should be smooth and spherical. The neutron wavelength was set to 6 or 12 Å ± 13.2% $\left(\frac{\Delta\lambda}{\lambda}\right)$. A 14 mm diameter circular aperture defined the size of the beam at the sample position. A dual detector system was used with the main detector positioned at 15.5 m from the sample and a curved west wing detector at 1.4° from the direct beam. Measurements using two instrument settings, one at 6 Å and another at 12 Å, together provided a continuous range of momentum transfer values $q$ from 0.0015 to 0.8 Å$^{-1}$. Momentum transfer, $q$, is defined as $q = \frac{4\pi}{\lambda}\sin\left(\frac{\theta}{2}\right)$, where $\theta$ is the scattering angle, i.e., the angle between the main and scattered neutron beams. Data reduction was performed using the facility-developed reduction software "drtsans" to yield the absolute scattering cross sections as a function of $q$.[26]

Each liposome was prepared at 100% $D_2O$ and two different $D_2O$/$H_2O$ (v/v) ratios of 80/20 and 60/40. In the case of the PS latex samples, the maximum composition of $D_2O$ was 90% because the stock suspension was already in $H_2O$. The contrast variation method provides us the validation on the presumed model and yields more accurate dimension through the simultaneous fitting for all three contrasts using the same structural parameters. The concentrations of ULVs and PS Latex suspensions tested by SANS were 5 and 10 mg/mL, respectively.

The molecular volume, neutron scattering length density ($\rho_N$), and mass densities ($\rho$) of materials and solvents are given in Table 1. The $\rho_N$ values of the two hydrocarbon chains (tails) in DMPC and its headgroup, which also contains the glycerol backbone, were calculated individually based on estimated molecular volumes ($V$) using the data from the literature[27,28] and through the equation $\rho_N = \frac{\sum_i n_i b_i}{V}$ in which $n_i$ and $b_i$ represent the number and the *neutron* scattering length[29] of the $i$th atom of the molecule, respectively.

Samples tested by SANS are labeled with the notation of sample name, followed by the volume percentages of $D_2O$ in the solvent, e.g., Lipo-A-60 indicating the liposome (extruded using a 30 nm polycarbonate membrane) in a solvent mixture of 60% $D_2O$ and 40% $H_2O$. Note that ULVs extruded using a 30 and 50 nm polycarbonate membrane are denoted by Lipo-A and Lipo-B, respectively.

## RESULTS AND DISCUSSION

**Light Scattering (LS).** *Dynamic Light Scattering (DLS).* The field time autocorrelation function of 0.25 mg/mL samples and the distribution of the lag time were obtained (Figures S2 and S3) and further analyzed to attain the decay rate, Γ. The individual $D$ of each sample is estimated from the

**Table 1. Values of Molecular Volume, Density, and SLDs for Materials Tested in this Study**

| | volume (Å$^3$) | $\rho_N$ ($10^{-6}$ Å$^{-2}$) | | $\rho$ (g/cm$^3$) | $\rho_N$ ($10^{-6}$ Å$^{-2}$) | solvent (v/v)[a] | $\rho_N$ ($10^{-6}$ Å$^{-2}$) |
|---|---|---|---|---|---|---|---|
| DMPC | 1101 | 0.28 | $D_2O$ | 1.11 | 6.39 | $D_2O/H_2O$ (60/40) | 3.61 |
| DMPC head | 390 | 1.54 | $H_2O$ | 1.00 | −0.56 | $D_2O/H_2O$ (80/20) | 5.00 |
| DMPC tail | 711 | −0.41 | DMPC | 1.02[27] | 0.28 | $D_2O/H_2O$ (90/10) | 5.70 |
| | | | PS latex | 1.08[18] | 1.08 | | |

[a]Volume ratio of $D_2O$ to $H_2O$.



https://doi.org/10.1021/acs.langmuir.2c02420
Langmuir 2023, 39, 227−235

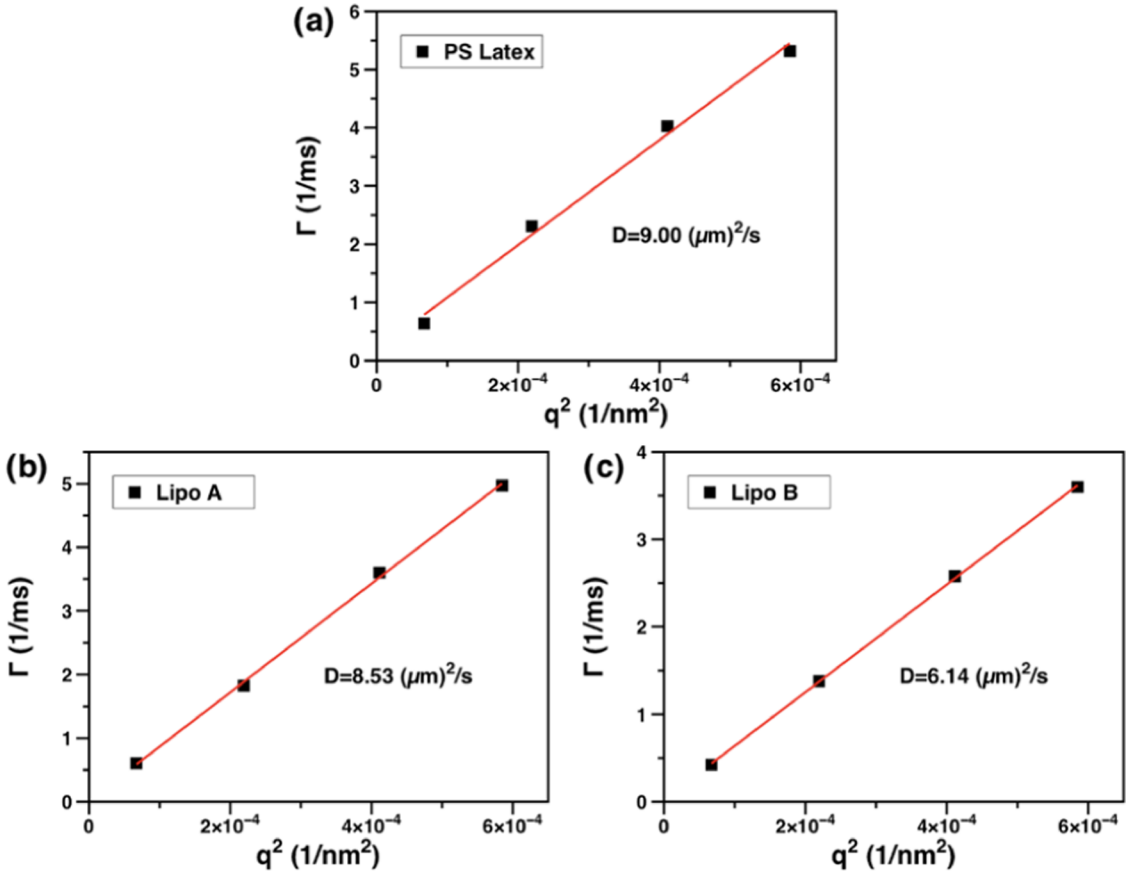


**Figure 2.** Decay rate, Γ, plotted against $q^2$ for (a) PS Latex, (b) Lipo-A, (c) Lipo-B at four different angles of 36, 68, 100, and 132° at 30 °C. *D* is the slope of the linear fit (red line) and is shown on the graphs.

**Table 2. SLS and DLS Outcome and Volume Fraction of Water in Nanoparticles**

| | $M$ (g/mol) | $V_{dry}$ (Å$^3$) | $R_h$(Å) | $V_{tot}$ (Å$^3$) | $\varphi^{LS}_{water}$ | $R_g^{exp}$(Å)[a] | $R_g^{cal}$ (Å)[b] |
|---|---|---|---|---|---|---|---|
| PS latex | (2.64 ± 0.07) × $10^7$ | (5.48 ± 0.84) × $10^7$ | 310 ± 20 | (1.25 ± 0.12) × $10^8$ | 0.56 ± 0.11 | 257 | 240 ± 16 |
| Lipo-A | (2.33 ± 0.11) × $10^7$ | (3.80 ± 0.18) × $10^7$ | 330 ± 10 | (1.51 ± 0.14) × $10^8$ | 0.75 ± 0.04 | 340 | 312 ± 87 |
| Lipo-B | (4.39 ± 0.49) × $10^7$ | (7.14 ± 0.79) × $10^7$ | 450 ± 10 | (3.82 ± 0.25) × $10^8$ | 0.81 ± 0.03 | 370 | 431 ± 112 |

[a] $R_g^{exp}$: The $R_g$ obtained by SLS experimentally. [b] $R_g^{cal}$: The calculated $R_g$ by replacing $R$ with $R_h$ in eqs 7 or 8.

slope of Γ versus $q^2$, as described in the Dynamic Light Scattering section and shown in Figure 2. From the Stokes–Einstein relationship (Dynamic Light Scattering), $R_h$ was calculated to be 330 ± 10, 450 ± 10, and 310 ± 20 Å for Lipo-A, Lipo-B, and PS Latex, respectively (Table 2).

*Static Light Scattering (SLS).* Figure 3 shows the Zimm plots of PS Latex, Lipo-A, and Lipo-B at four different concentrations (0.25, 0.5, 0.75, and 1.0 mg/mL), yielding the molar mass ($M$), which is derived from the common intercept of two lines obtained by extrapolating the data to $\theta = 0°$ and $c$ = 0 mg/mL (Table 2). The $M$ of PS Latex was estimated to be 2.640 × $10^7$ g/mol. $M$ for Lipo-A and Lipo-B, was estimated to be 2.333 × $10^7$ and 4.388 × $10^7$ g/mol, respectively.

*Estimation of Water Content by Light Scattering.* Following procedures in the Light Scattering section and with known kn densities of 1.02 and 0.8 g/cm$^3$ for DMPC[27] and PS Latex,[18] the dry and total volume of PS Latex, Lipo-A, and Lipo-B were estimated as shown in Table 2. The water content was estimated as 0.56 ± 0.11, 0.75 ± 0.04, and 0.81 ± 0.03 for PS Latex, Lipo-A, and Lipo-B, respectively, using eqs 4 and 5.

*SANS on PS Latex, Lipo-A, and Lipo-B.* To estimate the volume fraction of water ($\varphi_{water}$) associated with the NPs, the core–shell spherical (CSS) model (Supporting Information) was used to analyze the $\rho_N$ distribution of the NPs similar to our previous study[30] using SasView software. Figure 4a shows the best fits of PS Latex SANS data with three different $D_2O$/$H_2O$ solvent mixtures (60/40, 80/20, and 90/10) using the CSS model with identical structural parameters (i.e., shell thickness, core radius, and polydispersity). We hypothesize that the core is only made of hydrophobic PS with a more hydrophilic shell containing surfactant and water. Therefore, the scattering length density of core, $\rho_{N,core}$, and that of solvent, $\rho_{N,solv}$, were calculated and fixed for all samples (see Tables 1 and 3), while only the scattering length density of the shell, $\rho_{N,shell}$, was allowed to vary. Moreover, we applied simultaneous fitting for all samples of three contrasts with identical values of structural parameters (e.g., core radius, shell thickness, and polydispersity) since the variation of contrast should not change the NP structure. This chosen model can be validated if $\rho_{N,shell}$ is the only parameter to be adjusted for all of the best fits.


https://doi.org/10.1021/acs.langmuir.2c02420
Langmuir 2023, 39, 227–235

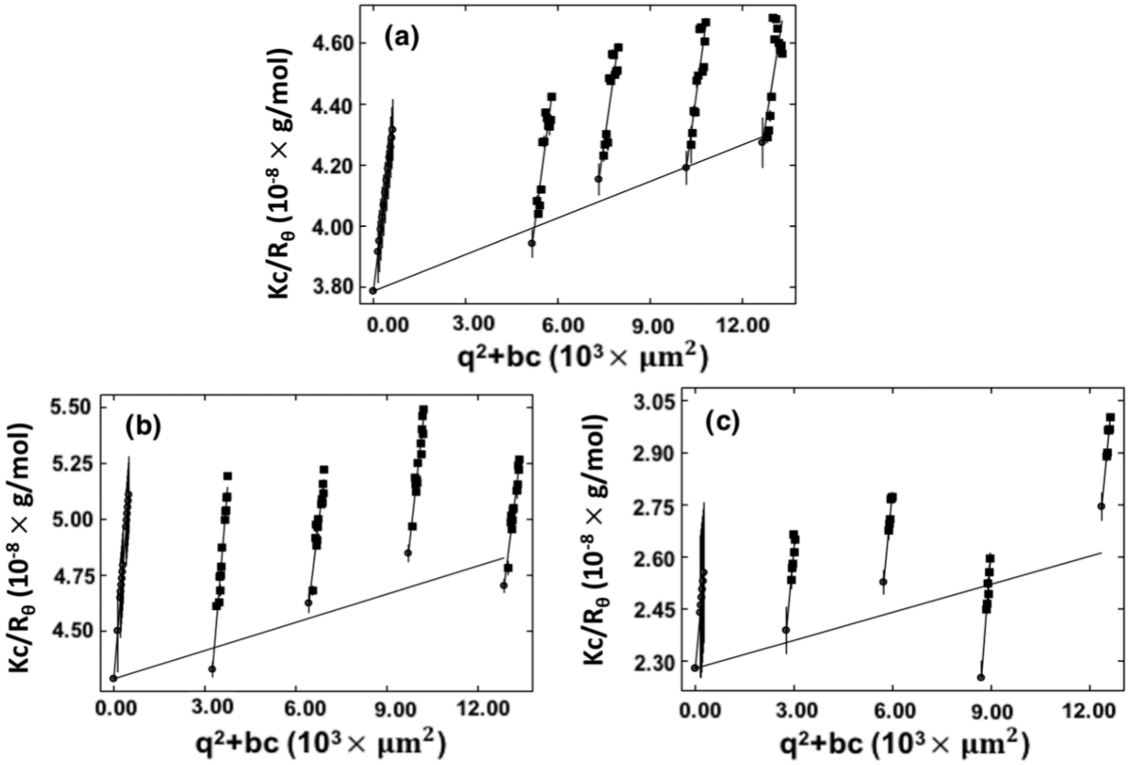


**Figure 3.** Zimm plot of (a) PS Latex, (b) Lipo-A, and (c) Lipo-B constructed by testing the samples at four different concentrations of 0.25, 0.5, 0.75, and 1 mg/mL and angles varying from 50 to 120° at 30 °C. Solid lines are linear fits leading to extrapolated points.

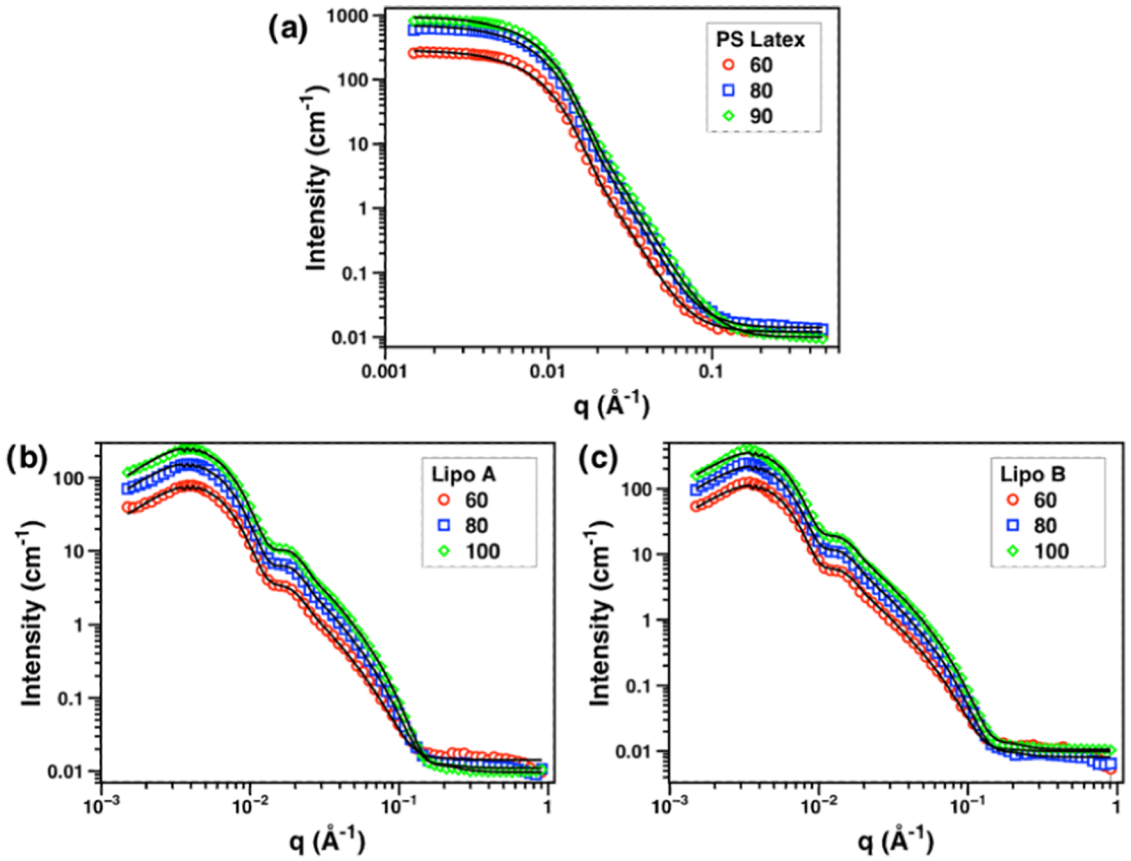


**Figure 4.** SANS data of (a) PS Latex, (b) Lipo-A, and (c) Lipo-B and their best fits. PS Latex is fit using the CSS model and Lipo-A and Lipo-B are fit by a combination of vesicle model and H-PMSA structure factor.



https://doi.org/10.1021/acs.langmuir.2c02420
*Langmuir* 2023, 39, 227−235

Table 3. SANS Fitting Outcome of PS Latex, Lipo-A, and Lipo-B along with the Estimated Volume Fraction of Water ($\varphi_{water}^{SANS}$)

| | core radius (Å) | shell thickness (Å) | total radius ($R_{SANS}$) (Å) | $\rho_{N,core}$ ($10^{-6}$ Å$^{-2}$) | $\rho_{N,shell}$ ($10^{-6}$ Å$^{-2}$) | $\varphi_{water}^{SANS}$ | $\chi^{2a}$ |
|---|---|---|---|---|---|---|---|
| PS latex 60 | | | | | 3.50 ± 0.02 | | |
| PS latex 80 | 182 ± 1 | 39 ± 1 | 221 ± 2 | 1.08 | 4.70 ± 0.02 | 0.42 ± 0.05 | 0.8 |
| PS latex 90 | | | | | 5.50 ± 0.02 | | |
| Lipo-A-60 | | | | 3.61 | 0.70 ± 0.01 | | |
| Lipo-A-80 | 195 ± 1 | 37 ± 1 | 232 ± 2 | 5.00 | 0.91 ± 0.01 | 0.65 ± 0.03 | 0.14 |
| Lipo-A-100 | | | | 6.39 | 1.10 ± 0.01 | | |
| Lipo-B-60 | | | | 3.61 | 0.68 ± 0.01 | | |
| Lipo-B-80 | 261 ± 1 | 39 ± 1 | 300 ± 2 | 5.00 | 0.92 ± 0.01 | 0.72 ± 0.03 | 0.33 |
| Lipo-B -100 | | | | 6.39 | 1.17 ± 0.01 | | |

[a] $\chi^2 \equiv \frac{1}{N}\sum_{i=1}^{N}\frac{(I_{exp}(q_i) - I_{model}(q_i))^2}{I_{exp}(q_i)}$, where $N$ is the total number of data points and $I_{exp}(q_i)$ and $I_{model}(q_i)$ are the experimental and calculated intensities at $q_i$, respectively.

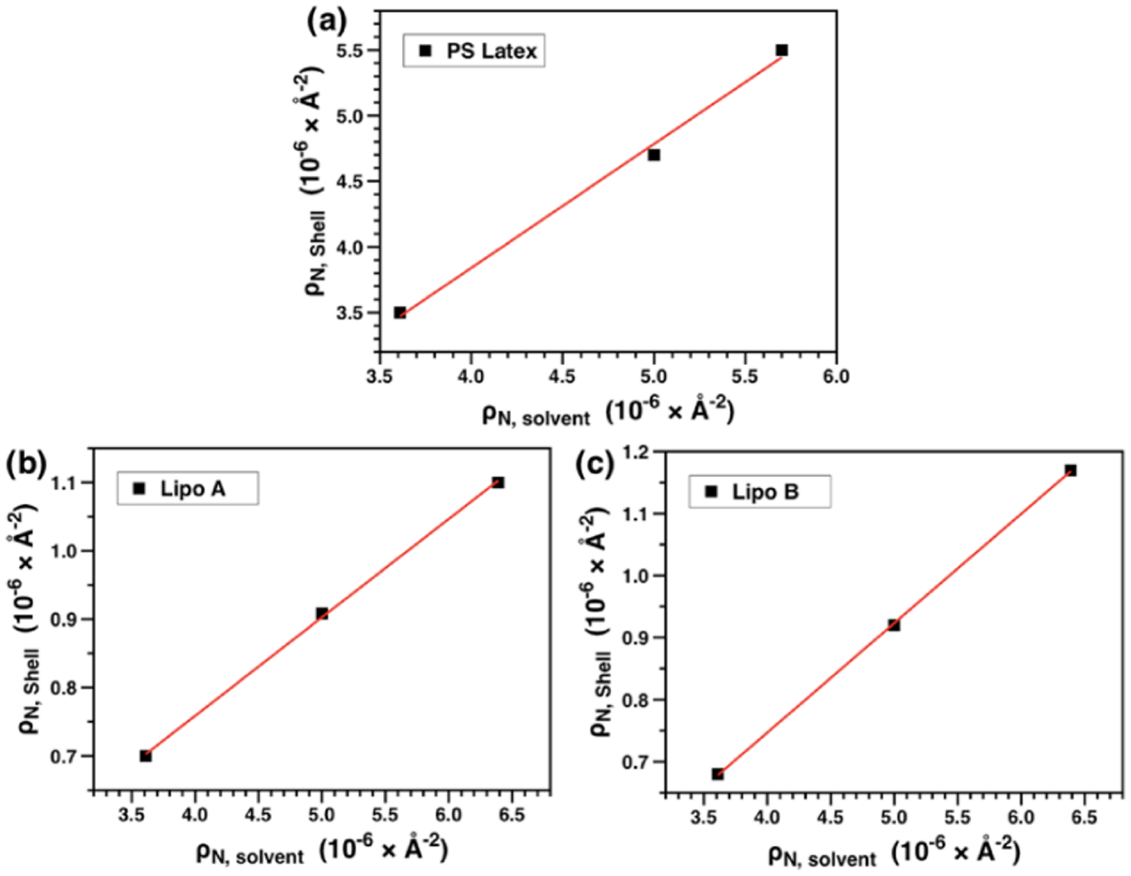


**Figure 5.** Plots of $\rho_{N,shell}$ vs $\rho_{N,solv}$ of (a) PS Latex, (b) Lipo-A, and (c) Lipo-B. Note that in the case of ULVs, shell is considered as the whole bilayer. Data are fit with a linear function (red line) and the slope of the linear fit yields the volume fraction of water inside the shell.

The fitting results (Table 3) suggest that a dry polystyrene core has a radius of 182 Å and an interfacial shell thickness of 39 Å. Note that only the shell contains water, and therefore, the SLD of the shell, $\rho_{N,shell}$, can be expressed as

$$\rho_{N,shell} = \rho_{N,dry}.\ (1 - \nu_{solv}) + \rho_{N,solv}.\ \nu_{solv} \quad (6)$$

where $\rho_{N,dry}$ represents the neutron scattering length density of the dry (before solvation) components, $\rho_{N,solv}$ can be calculated based on the composition of $D_2O$ and $H_2O$ of the solvent, and $\nu_{solv}$ represents the volume fraction of solvent molecules *inside the shell*. Equation 6 suggests that the best fit to $\rho_{N,shell}$ value (listed in Table 3) should have a linear relationship with $\rho_{N,solv}$ (listed in Table 1). Therefore, the contrast variation SANS experiment provides a powerful method to identify the internal hydration level of each part of the NPs (e.g., core and shell) from the slope of $\rho_{N,shell}$ plotted against $\rho_{N,solv}$ as shown in Figure 5 ($\nu_{solv}$ = 0.94 ± 0.06). The highly hydrated shell of the PS Latex is presumably due to the presence of surfactants and sulfate functional groups on the surface of the particles. When normalized by the total NP, the overall water content of a PS Latex nanoparticle is 0.42 ± 0.05.

Figure 4b,c illustrates the SANS data of Lipo-A and Lipo-B (with higher charge density, i.e., $R$ = 0.01), respectively. As a


https://doi.org/10.1021/acs.langmuir.2c02420
Langmuir 2023, 39, 227−235

result, the vesicle model (the CSS model with water associated with the core) was combined with the H-PMSA structure factor[22−24] to fit the SANS data. The broad peak at ∼0.003 Å$^{-1}$ is the result of Coulombic repulsion between neighboring vesicle particles, which is accounted for by the H-PMSA structure factor. Again, like the PS Latex samples, simultaneous fitting was employed to analyze the contrast variation series of SANS data of Lipo-A and Lipo-B. The $\rho_{N,core}$ was set equal to the corresponding solvent based on the calculated value during the fitting process (see Tables 1 and 3), and the $\rho_{N,shell}$ was allowed to vary due to the association of water with the polar groups of the bilayer. The hydration of the bilayer shell was obtained from Figure 5b,c as described for the case of PS Latex.

According to the best fitting results, liposomes have a bilayer thickness of approximately 37−39 Å at 30 °C, in agreement with previous studies,[15,31,32] and the best fitting core radii are 195 and 261 Å for Lipo-A and Lipo-B, respectively. Furthermore, the derived hydration fraction of the shell is 0.14 ± 0.01 and 0.18 ± 0.01 for Lipo-A and Lipo-B, respectively. These values are in good agreement with other reports, in which the volume fraction of water associated with the phosphate groups of DMPC ULVs was 0.19 ± 0.01[16] and 0.2 ± 0.05.[15] As a result, the volume fraction of water of the entire liposome (including the core and shell) was estimated to be 0.65 ± 0.03 and 0.72 ± 0.03 for Lipo-A and Lipo-B, respectively.

The water contents from SLS/DLS measurements are in good agreement with those from the SANS study (Tables 2 and 3). The discrepancy in the PS Latex NP total radius between DLS ($R_h$ = 310 Å) and SANS (221 Å) measurements is most likely attributed to the differences in which the two techniques measure. De Mel et al. have also reported that the size of DOPC vesicles measured by DLS was approximately 100 Å greater than the SANS estimation.[8] The derivation of $R_h$ is closely related to the mobility of the NP, while the size obtained from SANS analysis mainly depends on the morphology and contrast. One can imagine that any surface-associated water will affect the mobility of the NP, causing $R_h$ to appear larger than its actual size.[33−35] It should also be noted that for polydisperse NPs or suspensions with small fractions of larger particles (if they are outside the SANS probing range), the intensity-weighted $R_h$ can be biased toward the larger particles.[8,36−39] In either scenario (i.e., surface-associated water or over-sized particles for SANS), the total volume of NP is overestimated, leading to a lower volume fraction of the dry component and hence a high $\varphi_{water}$. This reasoning would also apply to the Lipo-A and Lipo-B samples. However, it should also be noted that the liposomes tested by LS have lower charge density than those in the SANS studies and they were also prepared in different batches. As a result, some variation in the sizes of the NPs is expected. However, we were able to make the lower charge density Lipo-A with a $R_h$ (330 Å) from DLS closer to the total radius of higher charge density Lipo-B (300 Å) based on the SANS analysis. The fact that the analyses of these two NPs yield similar water contents (75% of Lipo-A versus 72% of Lipo-B) further validates the SLS/DLS approach.

Further investigation on $R_g$ validates the accuracy of SLS/DLS data used for probing water content. First, the theoretical $R_g$ of NPs for solid or hollow spheres can be calculated by eqs 7 and 8, respectively, where $R$ and $R_i$ are the outer radius and inner radius, respectively. A solid sphere is a special condition ($R_i$ = 0) of eq 8, leading to eq 7.

$$\langle R_g^2 \rangle^{1/2} = \sqrt{3/5}\ R \tag{7}$$

$$\langle R_g^2 \rangle^{1/2} = \sqrt{\left(\frac{3}{5}\right)\frac{R^5 - R_i^5}{R^3 - R_i^3}} \tag{8}$$

Here, we replace $R$ with $R_h$ from the DLS measurements. For Lipo-A and Lipo-B, $R_i$ can be calculated by subtracting the bilayer thickness obtained from SANS (∼40 Å) from $R$, while $R_i$ is set to be 0 in the case of PS Latex NPs. The calculated $R_g$ ($R_g^{cal}$) is found to be 240 ± 16, 312 ± 87, and 431 ± 112 Å for PS Latex NPs, Lipo-A, and Lipo-B, respectively, in good agreement with the values of $R_g^{exp}$, the experimental $R_g$ obtained through the Zimm plots (Table 2).

The results of this study suggest that the SLS/DLS approach slightly overestimates the water content of NPs. This is because $R_h$ is larger than the actual external radius, $R$. Hence, the SLS/DLS method provides a good upper bound value for the water content, while SANS data provide an $R$ value that is closer to reality.

## CONCLUSIONS

We demonstrated two independent approaches (i.e., SLS/DLS and contrast variation SANS) to probe the water content of NPs. We pioneer the highly accessible SLS/DLS combined approach for such a study. Moreover, due to the long wavelength, light scattering approach is suitable to characterize particles >100 nm in radius. However, SLS/DLS is limited to the study of spherical particles, and the water content is, most likely, overestimated due to the surface-associated water, resulting in a difference between $R_h$ and $R$. In principle, contrast variation SANS is better at providing internal NP structural information due to its differential sensitivity between the protiated and deuterated species making up the NPs and does not require spherical particle geometry. However, in the case of SANS, the largest diameter NP that can be studied is limited by the lowest attainable $q$. In this study, since the radii of all three NPs were smaller than 60 nm, SANS was able to determine water content rather accurately. As a result of the need for much concentrated SANS samples, compared to SLS/DLS, the structure factor arising from interparticle interaction (e.g., highly charged particles or high concentration) adds another level of complication but is easily addressed with the use of appropriate structure factor to fit the data. Importantly, this report validates a more accessible approach for probing the water content of NPs with good accuracy, which should accelerate the development of new NPs.

## ASSOCIATED CONTENT

### Supporting Information

The Supporting Information is available free of charge at https://pubs.acs.org/doi/10.1021/acs.langmuir.2c02420.

Supporting information includes refractive index increment results (d$n$/d$c$), field correlation function, and lag time distribution obtained from DLS and quantitative description of core−shell sphere and vesicle model (PDF)



https://doi.org/10.1021/acs.langmuir.2c02420
Langmuir 2023, 39, 227−235

## AUTHOR INFORMATION


### Corresponding Author

**Mu-Ping Nieh** − *Polymer Program, Institute of Materials Science, University of Connecticut, Storrs, Connecticut 06269, United States; Materials Science Program, Institute of Materials Science, Department of Biomedical Engineering, and Department of Chemical and Biomolecular Engineering, University of Connecticut, Storrs, Connecticut 06269, United States;* orcid.org/0000-0003-4462-8716; Email: mu-ping.nieh@uconn.edu

### Authors

**Behrad Kangarlou** − *Materials Science Program, Institute of Materials Science, University of Connecticut, Storrs, Connecticut 06269, United States*

**Donyeil Hoy** − *Department of Biomedical Engineering, University of Connecticut, Storrs, Connecticut 06269, United States*

**Haden L. Scott** − *Neutron Scattering Division and Shull Wollan Center, Oak Ridge National Laboratory, Oak Ridge, Tennessee 37831, United States*

**Sai Venkatesh Pingali** − *Neutron Scattering Division, Oak Ridge National Laboratory, Oak Ridge, Tennessee 37831, United States;* orcid.org/0000-0001-7961-4176

**Nora Khalil** − *Department of Chemical and Biomolecular Engineering, University of Connecticut, Storrs, Connecticut 06269, United States;* Present Address: Department of Chemical Engineering, Northeastern University, Boston, Massachusetts 02115, United States

**Benjamin Chung** − *Department of Molecular and Cell Biology, University of Connecticut, Storrs, Connecticut 06269, United States*

**John Katsaras** − *Neutron Scattering Division and Shull Wollan Center, Oak Ridge National Laboratory, Oak Ridge, Tennessee 37831, United States;* orcid.org/0000-0002-8937-4177

Complete contact information is available at: https://pubs.acs.org/10.1021/acs.langmuir.2c02420

### Author Contributions

[▽]B.K. and D.H. contributed equally. The manuscript was written through contribution of all authors.


### Notes

The authors declare no competing financial interest.

This manuscript has been coauthored by UT-Battelle, LLC, under Contract No. DE-AC05- 00OR22725 with the U.S. Department of Energy. The United States Government retains and the publisher, by accepting the article for publication, acknowledges that the United States Government retains a non-exclusive, paid-up, irrevocable, world-wide license to publish or reproduce the published form of this manuscript, or allow others to do so, for United States Government purposes. The Department of Energy will provide public access to these results of federally sponsored research in accordance with the DOE Public Access Plan (http://energy.gov/downloads/doe-public-access-plan).

## ACKNOWLEDGMENTS

H.L.S. and J.K. were supported through the Scientific User Facilities Division of the DOE Office of Basic Energy Sciences under US DOE Contract No. DE-AC05-00OR22725. Neutron scattering studies performed on CG-3 Bio-SANS (IPTS-28955.1) and S.V.P are supported by the Office of Biological and Environmental Research funded Center for Structural Molecular Biology (CSMB) under Contract FWP ERKP291, using the High Flux Isotope Reactor supported by the Scientific User Facilities Division, Office of Basic Energy Sciences, U.S. Department of Energy. The SANS/SAXS data were fitted utilizing the SasView 4.2.2 application, originally developed under NSF award DMR-0520547. SasView contains code developed with funding from the European Union's Horizon 2020 research and innovation programme under the SINE2020 project, grant agreement No. 654000.

## REFERENCES


(1) Sebastiani, F.; Arteta, M. Y.; Lerche, M.; Porcar, L.; Lang, C.; Bragg, R. A.; Elmore, C. S.; Krishnamurthy, V. R.; Russell, R. A.; Darwish, T.; Pichler, H.; Waldie, S.; Moulin, M.; Haertlein, M.; Forsyth, V. T.; Lindfors, L.; Cárdenas, M. Apolipoprotein E Binding drives structural and compositional rearrangement of mRNA containing lipid nanoparticles. *ACS Nano* **2021**, *15*, 6709−6722.

(2) Brader, M. L.; Williams, S. J.; Banks, J. M.; Hui, W. H.; Zhou, Z. H.; Jin, L. Encapsulation state of messenger RNA inside lipid nanoparticles. *Biophys. J.* **2021**, *120*, 2766−2770.

(3) Kim, J.; Eygeris, Y.; Gupta, M.; Sahay, G. Self-assembled mRNA vaccines. *Adv. Drug Delivery Rev.* **2021**, *170*, 83−112.

(4) Zhang, Y.; Sun, C.; Wang, C.; Jankovic, K. E.; Dong, Y. Lipids and lipid derivatives for RNA delivery. *Chem. Rev.* **2021**, *121*, 12181−12277.

(5) Schoenmaker, L.; Witzigmann, D.; Kulkarni, J. A.; Verbeke, R.; Kersten, G.; Jiskoot, W.; Crommelin, D. J. A. mRNA-lipid nanoparticle COVID-19 vaccines: structure and stability. *Int. J. Pharm.* **2021**, *601*, No. 120586.

(6) Fabre, A.-L.; Colotte, M.; Luis, A.; Tuffet, S.; Bonnet, J. An efficient method for long-term room temperature storage of RNA. *Eur. J. Hum. Genet.* **2014**, *22*, 379−385.

(7) Qian, S.; Sharma, V. K.; Clifton, L. A. Understanding the structure and dynamics of complex biomembrane interactions by neutron scattering techniques. *Langmuir* **2020**, *36*, 15189−15211.

(8) De Mel, J. U.; Gupta, S.; Harmon, S.; Stingaciu, L.; Roth, E. W.; Siebenbuerger, M.; Bleuel, M.; Schneider, G. J. Acetaminophen interactions with phospholipid vesicles induced changes in morphology and lipid dynamics. *Langmuir* **2021**, *37*, 9560−9570.

(9) Berlinger, S. A.; Chen, X.; Yutkin, M.; Radke, C. J. A two-phase model for adsorption from solution using quartz crystal microbalance with dissipation. *Langmuir* **2022**, *38*, 10114−10127.

(10) Biswas, S.; Melton, L. D.; Nelson, A. R. J.; Le Brun, A. P.; Heinrich, F.; McGillivray, D. J.; Xu, A. Y. The assembly mechanism and mesoscale architecture of protein−polysaccharide complexes formed at the solid−liquid interface. *Langmuir* **2022**, *38*, 12551−12561.

(11) Sebastiani, F.; Arteta, M. Y.; Lindfors, L.; Cárdenas, M. Screening of the binding affinity of serum proteins to lipid nanoparticles in a cell free environment. *J. Colloid Interface Sci.* **2022**, *610*, 766−774.

(12) Vermette, P.Liposome characterization by quartz crystal microbalance measurements and atomic force microscopy. In *Methods Enzymol*; Duzgunes, N., Ed.; Elsevier, 2009; Vol. *465*, pp 43−73.

(13) Kulkarni, J. A.; Darjuan, M. M.; Mercer, J. E.; Chen, S.; Meel, R. v. d.; Thewalt, J. L.; Tam, Y. Y. C.; Cullis, P. R. On the formation and morphology of lipid nanoparticles ontaining ionizable cationic lipids and siRNA. *ACS Nano* **2018**, 4787−4795.

(14) Kulkarni, J. A.; Witzigmann, D.; Leung, J.; Tam, Y. Y. C.; Cullis, P. R. On the role of helper lipids in lipid nanoparticle formulations of siRNA. *Nanoscale* **2019**, *11*, 21733−21739.

(15) Balgavý, P.; Dubničková, M.; Kučerka, N.; Kiselev, M. A.; Yaradaikin, S. P.; Uhríková, D. Bilayer thickness and lipid interface area in unilamellar extruded 1,2-diacylphosphatidylcholine liposomes: a small-angle neutron scattering study. *Biochim. Biophys. Acta, Biomembr.* **2001**, *1512*, 40−52.

(16) Kučerka, N.; Kiselev, M. A.; Balgavy, P. Determination of bilayer thickness and lipid surface area in unilamellar dimyristoylphosphatidylcholine vesicles from small-angle neutron scattering curves: a comparison of evaluation methods. *Eur. Biophys. J.* **2004**, *33*, 328−334.
(17) Arteta, M. Y.; Kjellman, T.; Bartesaghi, S.; Wallin, S.; Wu, X.; Kvist, A. J.; Dabkowska, A.; Székely, N.; Radulescu, A.; Bergenholtz, J.; Lindfors, L. Successful reprogramming of cellular protein production through mRNA delivered by functionalized lipid nanoparticles. *Proc. Natl. Acad. Sci. U.S.A.* **2018**, *115*, E3351−E3360.
(18) Gao, J.; Zhou, S.; Wu, C. Characterization of spherical microlatex particles made of linear uncrosslinked polystyrene chains. *Polym. Eng. Sci.* **1996**, *36*, 2968−2972.
(19) Wu, C.; Chan, K. K. Laser light-scattering investigation of the density of pauci-chain polystyrene microlatices. *J. Polym. Sci., Part B: Polym. Phys.* **1995**, *33*, 919−925.
(20) Wu, C.; Chan, K. K.; Woo, K. F.; Qian, R.; Li, X.; Chen, L.; Napper, D. H.; Tan, G.; Hill, A. J. Characterization of pauci-chain polystyrene microlatex particles prepared by chemical initiator. *Macromolecules* **1995**, *28*, 1592−1597.
(21) Scott, H. L.; Skinkle, A.; Kelley, E. G.; Waxham, M. N.; Levental, I.; Heberle, F. A. On the mechanism of bilayer separation by extrusion, or why your LUVs Are not really unilamellar. *Biophys. J.* **2019**, *117*, 1381−1386.
(22) Hansen, J.-P.; Hayter, J. B. A rescaled MSA structure factor for dilute charged colloidal dispersions. *Mol. Phys.* **1982**, *46*, 651−656.
(23) Hayter, J. B.; Penfold, J. An analytic structure factor for macroion solutions. *Mol. Phys.* **1981**, *42*, 109−118.
(24) Hayter, J. B.; Penfold, J. Determination of micelle structure and charge by neutron small-angle scattering. *Colloid Polym. Sci.* **1983**, *261*, 1022−1030.
(25) Heller, W. T.; Urban, V. S.; Lynn, G. W.; Weiss, K. L.; O'Neill, H. M.; Pingali, S. V.; Qian, S.; Littrell, K. C.; Melnichenko, Y. B.; Buchanan, M. V.; Selby, D. L.; Wignall, G. D.; Butler, P. D.; Myles, D. A. The Bio-SANS instrument at the High Flux Isotope Reactor of Oak Ridge National Laboratory. *J. Appl. Crystallogr.* **2014**, *47*, 1238−1246.
(26) Heller, W. T.; Hetrick, J.; Bilheux, J.; Borreguero Calvo, J. M.; Chen, W.-R.; DeBeer-Schmitt, L.; Do, C.; Doucet, M.; Fitzsimmons, M. R.; Godoy, W. F.; Granroth, G. E.; Hahn, S.; He, L.; Islam, F.; Lin, J.; Littrell, K. C.; McDonnell, M.; McGaha, J.; Peterson, P. F.; Pingali, S. V.; Qian, S.; Savici, A. T.; Shang, Y.; Stanley, C. B.; Urban, V. S.; Whitfield, R. E.; Zhang, C.; Zhou, W.; Billings, J. J.; Cuneo, M. J.; Ferraz Leal, R. M.; Wang, T.; Wu, B. drtsans: The data reduction toolkit for small-angle neutron scattering at Oak Ridge National Laboratory. *SoftwareX* **2022**, *19*, No. 101101.
(27) Nagle, J. F.; Wilkinson, D. A. Lecithin bilayers density measurements and molecular interactions. *Biophys. J.* **1978**, *23*, 159−175.
(28) Kučerka, N.; Liu, Y.; Chu, N.; Petrache, H. I.; Tristram-Nagle, S.; Nagle, J. F. Structure of fully hydrated fluid phase DMPC and DLPC lipid bilayers using X-ray scattering from oriented multilamellar arrays and from unilamellar vesicles. *Biophys. J.* **2005**, *88*, 2626−2637.
(29) Sears, V. F. Neutron scattering lengths and cross sections. *Neutron News* **1992**, *3*, 26−37.
(30) Kangarlou, B.; Dahanayake, R.; Martin, I. J.; Ndaya, D.; Wu, C.-M.; Kasi, R. M.; Dormidontova, E. E.; Nieh, M.-P. Flower-like micelles of polyethylene oxide end-capped with cholesterol. *Macromolecules* **2021**, *54*, 8960−8970.
(31) Gallová, J.; Uhríková, D.; Kučerka, N.; Doktorovová, S.; S Funari, S.; Teixeira, J.; Balgavy′, P. The effects of cholesterol and b-sitosterol on the structur of saturated diacylphosphatidylcholine bilayers. *Eur. Biophys. J.* **2011**, *40*, 153−163.
(32) Pencer, J.; Nieh, M.-P.; Harroun, T. A.; Krueger, S.; Adams, C.; Katsaras, J. Bilayer thickness and thermal response of dimyristoylphosphatidylcholine unilamellar vesicles containing cholesterol, ergosterol and lanosterol: A small-angle neutron scattering study. *Biochim. Biophys. Acta, Biomembr.* **2005**, *1720*, 84−91.
(33) Thomä, S. L. J.; Krauss, S. W.; Eckardt, M.; Chater, P.; Zobe, M., Atomic insight into hydration shells around facetted nanoparticles. *Nat. Commun.***2019**, *10* DOI: 10.1038/s41467-019-09007-1.
(34) Nigro, V.; Angelini, R.; King, S.; Franco, S.; Buratti, E.; Bomboi, F.; Mahmoudi, N.; Corvasce, F.; Scaccia, R.; Church, A.; Charleston, T.; Ruzicka, B. Apparatus for simultaneous dynamic light scattering−small angle neutron scattering investigations of dynamics and structure in soft matter. *Rev. Sci. Instrum.* **2021**, *92*, No. 023907.
(35) Mahl, D.; Diendorf, J.; Meyer-Zaika, W.; Epple, M. Possibilities and limitations of different analytical methods for the size determination of a bimodal dispersion of metallic nanoparticles. *Colloids Surf., A* **2011**, *377*, 386−392.
(36) Bouanani, F.; Bendedouch, D.; Teixeira, J.; Marx, L.; Hemery, P. Characterization of a miniemulsion by DLS and SANS. *Colloids Surf., A* **2012**, *404*, 47−51.
(37) Fissan, H.; Ristig, S.; Kaminski, H.; Asbach, C.; Epple, M. Comparison of different characterization methods for nanoparticle dispersions before and after aerosolization. *Anal. Methods* **2014**, *6*, 7324−7334.
(38) Malm, A. V.; Corbett, J. C. W. Improved dynamic light Scattering using an adaptive and statistically driven time resolved treatment of correlation data. *Sci. Rep.* **2019**, *9*, No. 13519.
(39) Adkins, G. B.; Sun, E.; Coreas, R.; Zhong, W. Asymmetrical flow field flow fractionation coupled to nanoparticle tracking analysis for rapid online characterization of nanomaterials. *Anal. Chem.* **2020**, *92*, 7071−7078.

## Recommended by ACS

**Molecular Dynamics Simulation Studies of Bile, Bile Salts, Lipid-Based Drug Formulations, and mRNA–Lipid Nanoparticles: A Review**
Amali G. Guruge, David K. Chalmers, *et al.*
MAY 17, 2023
MOLECULAR PHARMACEUTICS
READ

**Role of Residual Monomers in the Manifestation of (Cyto)toxicity by Polystyrene Microplastic Model Particles**
Yuanhu Zhang, Andreas Greiner, *et al.*
JUNE 26, 2023
ENVIRONMENTAL SCIENCE & TECHNOLOGY
READ

**Effect of Albumin Corona Conformation on *In Vitro* and *In Vivo* Profiles of Intravenously Administered Nanoparticles**
Beibei Wu, Yao Fu, *et al.*
APRIL 28, 2023
MOLECULAR PHARMACEUTICS
READ

**Identification of the Proteins Determining the Blood Circulation Time of Nanoparticles**
Cintia Marques, Lionel Maurizi, *et al.*
JUNE 28, 2023
ACS NANO
READ

Get More Suggestions >


https://doi.org/10.1021/acs.langmuir.2c02420
*Langmuir* 2023, 39, 227−235